Short lifetimes in mirror nuclei ^{25}Mg-^{25}Al

P. Tikkanen, J. Keinonen, and A. Kangasmäki
Accelerator Laboratory, University of Helsinki, Hämeentie 100, SF-00550 Helsinki, Finland

Zs. Fülöp, Á.Z. Kiss, and E. Somorjai
Institute of Nuclear Research of the Hungarian Academy of Sciences, P.O. Box 51, H-4001 Debrecen, Hungary

(Received 25 January 1991)

Mean lifetimes of levels in the mirror nuclei ^{25}Mg and ^{25}Al have been measured using the Doppler-shift-attenuation (DSA) method and the reactions ^{12}C(^{15}N,pn)^{25}Mg and ^{24}Mg(p,γ)^{25}Al, respectively. The lifetime values or limits were determined for 13 bound levels in ^{25}Mg below the excitation energy of 7 MeV and for the 1.61- and 1.79-MeV bound levels in ^{25}Al. The lifetime values or limits of the 7.79, 8.02, and 9.00 MeV neutron unbound states in ^{25}Mg, and the 2.72-, 3.42-, and 4.03-MeV proton unbound states in ^{25}Al were also determined. The lifetimes of four levels in ^{25}Mg are reported for the first time. The targets were prepared by implanting ^{12}C and ^{24}Mg into Ta substrates, to ensure effective slowing down of the recoils. Computer simulations with the Monte Carlo method and experimental stopping power were used in the DSA analysis. Experimental transition matrix elements, based on the measured mean lifetime values, are compared with predictions of the universal *sd*-shell model.

I. INTRODUCTION

The nucleus ^{25}Mg is one of the first examples on strongly deformed nuclei in the *sd*-shell region. Low-lying levels were interpreted by Litherland *et al.*[1] to exhibit the rotational spectrum of a prolate nucleus. The excitation spectrum has been studied extensively up to 6.1 MeV with light-ion beams in the intervening years.[2,3] Headly *et al.*[4] have recently made the first heavy-ion study of ^{25}Mg and extended the ground-state rotational band up to spin $J^\pi = \frac{15}{2}^+$. Comparison with the universal *sd*-shell model[5] (USD) and cranked Nilsson-Strutinski model[6] yielded good agreement between the shell model and experimental level energies and γ-decay branches while the cranking model provided a comprehensive description of the configuration in the yrast $\frac{11}{2}$, $\frac{13}{2}$, and $\frac{17}{2}$ states. The electromagnetic transition matrix elements, providing the most stringent testing ground for the wave functions, could not be compared since the lifetimes were not measured.

The present work is a continuation to our systematic study of the short lifetimes in the *sd*-shell nuclei using the improved Doppler-shift-attenuation (DSA) method as developed at the Helsinki University accelerator laboratory.[7–12] Recent work on large-basis multishell wave functions for the *sd*-shell nuclei[5,13,14] has revealed the necessity of such reliable and consistent lifetime data for the $M1$ and $E2$ transition strengths.

Previous to this experiment, only a few studies[2] have been reported in the literature on the lifetime values in the nucleus ^{25}Mg, the most extensive ones being based on the reactions ^{25}Mg($p,p'\gamma$)^{25}Mg and ^{24}Mg(d,p)^{25}Mg. For the mirror nucleus ^{25}Al the data are also scarce and the previously reported lifetime values in ^{25}Al are based mainly on the reaction ^{24}Mg(p,γ)^{25}Al. Most of the previously existing information on lifetimes in ^{25}Mg and ^{25}Al is based on DSA studies.[2] However, because a variety of evaporated targets with slow stopping powers were used in these studies of short lifetimes and because the slowing-down theory[15] was used in many instances without sufficient experimental confirmation, the reported values have large uncertainties and mutual inconsistencies.

This paper describes lifetime measurements in the mirror nuclei ^{25}Mg-^{25}Al using the improved DSA method through the heavy-ion reaction ^{12}C(^{15}N,pn)^{25}Mg and the capture reaction ^{24}Mg(p,γ)^{25}Al. The effective stopping power is obtained by using implanted ^{12}C and ^{24}Mg targets in Ta. In comparison with the previous lifetime measurements, this is an essential advantage in the determination of short nuclear lifetimes with the DSA method. Additional differences are the use of the experimentally known stopping power, the computer simulation of γ-ray line shapes with the Monte Carlo (MC) method and the consistent use of the same technique in the DSA analysis of the high recoil velocity [the reaction ^{12}C(^{15}N,pn)^{25}Mg] and low recoil velocity data [the reaction ^{24}Mg(p,γ)^{25}Al]. With this technique lifetime values of excited states in the mirror nuclei ^{25}Mg-^{25}Al could be determined to an accuracy which is sufficient to permit extraction of $M1$ and $E2$ transition matrix elements for a meaningful comparison with theoretical values.

II. EXPERIMENTAL ARRANGEMENTS

In the ^{12}C(^{15}N,pn)^{25}Mg reaction studies, 17 to 27 MeV ^{15}N beams of about 200 particle nA were supplied by the 5-MV tandem accelerator EGP-10-II of the Helsinki University accelerator laboratory. The beam spots were 2×2 mm^2 on the target. In the ^{24}Mg(p,γ)^{25}Al reaction studies, the 5-MV Van de Graaff accelerator of the Institute of Nuclear Research in Debrecen supplied 1.20 to 1.83 MeV proton beams of about 13 μA. The beams were collimated to form a spot of 5 mm in diameter on the target.

The ^{12}C targets were prepared by implanting a 20 μg/cm^2 fluence of 100-keV ^{12}C$^+$ ions into 0.4-mm-thick Ta sheets at the isotope separator of the Helsinki University accelerator laboratory. Also a low-density (ϱ = 0.09 g cm^{-3}) carbon target of 100 μg cm^{-2} thickness on a Ta backing was prepared.[8] The ^{24}Mg targets were prepared by implanting a 12 μg/cm^2 fluence of 60-keV ^{24}Mg$^+$ ions into 0.4-mm-thick Ta sheets at the isotope separator.

During the measurements, the ^{12}C target was set either perpendicular or at 45° relative to the beam. The target backing was directly air-cooled or the target holder made of copper was air-cooled. A vacuum better than 10 μPa was maintained in the target chamber to prevent carbon build-up. The ^{24}Mg target was set perpendicular to the beam in a target holder which provided direct water cooling of the Ta sheet.

The γ radiation resulting from target bombardment was detected in the ^{12}C(^{15}N,pn)^{25}Mg reaction measurements by a Princeton gamma-tech Ge(Li) and ORTEC HPGe detector, with efficiencies of 21.8% and 40%, respectively. The energy resolutions were 3.0 and 2.0 keV at E_γ = 1.33 MeV and 4.1 and 2.8 keV at E_γ = 2.61 MeV, respectively. In the ^{24}Mg(p,γ)^{25}Al reaction measurements, a 25% efficient ORTEC HPGe detector was used in the DSA measurements and a 20% efficient ORTEC HPGe detector in simultaneous branching ratio measurements. The energy resolutions of the detection systems were 2.2 and 2.3 keV at E_γ = 1.46 MeV and 3.0 and 3.2 keV at E_γ = 2.61 MeV, respectively. As during the course of this study a new ORTEC HPGe detector with an efficiency of 20% and energy resolution of 1.9 keV at E_γ = 1.46 MeV and 2.4 keV at E_γ = 2.61 MeV became available, most of the measurements were repeated. The detectors were shielded by a 6-cm-thick lead shield against the laboratory background radiation.

The γ-ray spectra were stored in a 4 or 8 K channel memory with dispersions of 0.37–2.0 keV/channel. The stability of spectrometers was checked with a ^{208}Tl γ-ray source and the ^{40}K laboratory background. The energy and efficiency calibrations of the γ-ray detectors were done with ^{56}Co sources[16] placed in the target position. The 6.13 MeV γ-ray line from ^{16}O was utilized in calibration of energies above 3.5 MeV in the ^{12}C(^{15}N,pn)^{25}Mg reaction study. The excited ^{16}O nuclei were produced in the reaction ^{19}F($p,\alpha\gamma$)^{16}O which took place in teflon materials in the target chamber.

III. MEASUREMENTS AND RESULTS

A. Stopping power

The stopping power of Ta for ^{25}Mg and ^{25}Al ions was described in the DSA analysis according to the following equation:

$$\left(\frac{dE}{dx}\right)_{\rm corr} = (0.67 \pm 0.05)\left(\frac{dE}{dx}\right)_n + \left(\frac{dE}{dx}\right)_e^{\rm exp}. \quad (1)$$

The uncorrected nuclear stopping power $(dE/dx)_n$ was calculated by the MC method, where the scattering angles of the recoiling ions were directly derived from the classical scattering integral[7] and the interatomic interaction was described by the universal potential (ZBL) given by Ziegler *et al.*[17] The correction parameter (0.67±0.05) for the nuclear stopping power of polycrystalline Ta for ^{25}Mg and ^{25}Al ions, was based on systematic studies on the nuclear stopping power at low velocities done in our laboratory.[7,18,19] The electronic stopping power $(dE/dx)_e^{\rm exp}$ of Ta for ^{25}Mg and ^{25}Al ions was deduced by correcting the recent experimental values obtained for ^{26}Mg ions slowing down in Ta (Ref. 20) for the differences in mass and Z values of the ions. The uncertainty of the electronic stopping power was estimated to be ±7%.

Based on our studies on the effect of implanted target atoms on the density of the backing material and lifetime values obtained by DSA,[7,8] along with the fluences of ^{12}C and ^{24}Mg, the implanted layers were assumed to have an insignificant effect on the density of Ta probed by $\beta \approx 0.03$ ^{25}Mg or 0.002 ^{25}Al recoils.

B. The ^{12}C(^{15}N,pn)^{25}Mg reaction study

The Doppler-shifted γ rays were detected at the angle 0° relative to the beam direction. The detector was located 4.0–8.0 cm from the target and was shielded from low energy γ rays and x rays by 4 mm of lead. The corrections for solid-angle attenuation of the observed Doppler shifts and for the finite initial velocity distribution were determined from fully shifted γ rays of short-lived states (τ < 10 fs) using the low-density carbon target on Ta with very low stopping power.[8] The first moments of the fully shifted γ-ray line shapes were utilized in obtaining accurate level energies for the short-lived states. The stopped component of the line shape was used in cases where it was clearly seen. The values of the deduced level energies are collected in Table I.

Figs. 1 and 2 show portions of the γ-ray spectra from the DSA measurements of the 3.97-, 4.06-, 5.53-, and 4.71-MeV states. The DSA analysis was performed by the computer simulation of γ-ray line shapes with the MC method.[7–12] In addition to the line shape, lifetimes were deduced by comparing the attenuated shift with the experimental full shift obtained using the low-density carbon target. A summary of the results is given in Table II. Several γ-ray peaks were included in the DSA analysis

TABLE I. Excitation energies of states in ^{25}Mg obtained in the present work and comparison with the previous values.

E_x (keV)		
Present	Previous	
	Ref. 2	Ref. 4
3405.2±0.3	3405.2±0.3	
3967.5±0.5	3970.7±0.3	
4059.9±0.5	4059.6±1.8	
5251.7±0.3	5251.3±0.3	
5460.3±0.2	5461.7±1.1	
5523.0±0.3	5520.9±0.4	
5530.4±0.5	5533.6±0.4	
6033.4±1.3	6041.3±0.5	
6862.2±1.2		6881±2
7791.0±1.5		7801±2
8016±2		8011±2
8818.5±0.7		8811±3
8999.5±1.5		9013±2

for each state when possible.

To control the effect of the feeding transitions on the γ-ray line shapes and deduced lifetime values, the measurements through the reaction ^{12}C(^{15}N,pn)^{25}Mg were performed at $E(^{15}\text{N})$ = 17, 20, 23 and 27 MeV. In the deduction of the lifetime values from the line shapes and from $F(\tau)$ values, the corrections for indirect feedings were obtained by measuring the population of the ^{25}Mg states at each energy of the nitrogen beam. The γ-ray decay schemes of the bound states in ^{25}Mg have been extensively studied in the literature.[2,4] A simulated line shape was obtained as the sum of the shapes corresponding to the direct prompt and delayed feeding of the state. The sum was weighted by the experimental fractions of the feedings. Uncertainties of the feeding lifetimes were those given in Table II for the adopted lifetimes. The feeding corrections are summarized in Table III.

The stopped component of the line shape correspond-

TABLE II. Summary of the lifetimes in ^{25}Mg obtained in the present work and comparison with the previously measured lifetime values.

E_x (MeV)	$E(^{15}\text{N})$ (MeV)	$F(\tau)$[a] (%)	τ[b] (fs)	τ[c](fs) adopted	τ (fs) (previous values) Refs. 21, 22	Ref. 23	Ref. 24	Others
1.96	17		1010±50	1010±80	1380±120		$600\pm^{180}_{100}$	
	20		$1010\pm^{75}_{45}$					
3.41	17	97.5±1.7	9±6	9±6	$10\pm^{6}_{4}$	$30\pm^{48}_{9}$	33±19	11.2±0.9[d]
	20	>98	<8					9.2±0.8[e]
	23	>99	<4					
	27	>98	<5					
3.91	27	98.2±1.0	9±3	9±3	<10	<10	<20	
3.97	23		35±8	36±7	46±22	$26\pm^{37}_{15}$	24±11	
	27		$36\pm^{6}_{5}$					
4.06	23	86.5±1.0	$80\pm^{5}_{3}$	80±6	$61\pm^{6}_{7}$	$49\pm^{69}_{29}$	53±10	75±8[d]
	27	88.3±0.5	80±3					76±6[e]
4.71	20		36±3	36±4	22±16	$42\pm^{46}_{38}$		
	23		37±3					
	27		35±4					
5.25	23	95.1±1.1	23±5	22±3	$20\pm^{5}_{4}$	<19		
	27	94.9±0.6	21±3					
5.46	27		2080±120	2080±190	4600±600	$1390\pm^{2060}_{900}$		
5.52	27		67±5	67±8		<10		
5.53	20	95.2±3.2	18±12	8±3	<10	<10		
	23	98.0±1.1	6±3					
	27	98.6±1.0	8±3					
5.75	23	>97	<10	<10	<10	<10		0.84±0.35[f]
	27	>98	<8					
6.03	23	>98	<8	<8	<39	<10		
	27	>98	<8					
6.86	27	>96	<13	<13				
7.79	27	>97	<10	<10				
8.02	27		53±4	53±5				
9.00	27	>96	<13	<13				

[a]Values have not been corrected for delayed feedings.
[b]Values given are corrected for feedings and are based on the $F(\tau)$ value and on the line-shape analysis. Only statistical errors are shown.
[c]Values include the uncertainty in the experimental stopping power.
[d]Reference 25. Inelastic electron scattering.
[e]Reference 26. Inelastic electron scattering.
[f]Reference 27. Inelastic electron scattering.

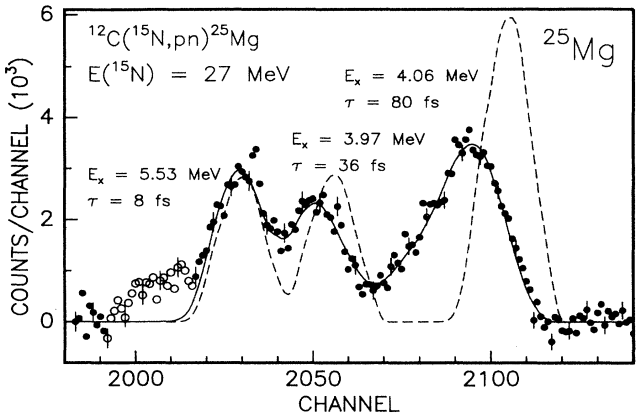

FIG. 1. Portion of γ-ray spectrum recorded in the DSA measurements of the 3.97-MeV (3.97 → 0 MeV transition), the 4.06-MeV (4.06 → 0 MeV transition), and the 5.53-MeV (5.53 → 1.61 MeV transition) ^{25}Mg states. The solid line is the sum of the three simulated line shapes for the shown lifetimes of the states; τ(3.97) = 36±7 fs, τ(4.06) = 80±6 fs, τ(5.53) = 8±3 fs. The dashed line is the sum of the three simulated line shapes for the low-density carbon target. The contamination peak denoted by open circles was excluded in the line-shape fitting.

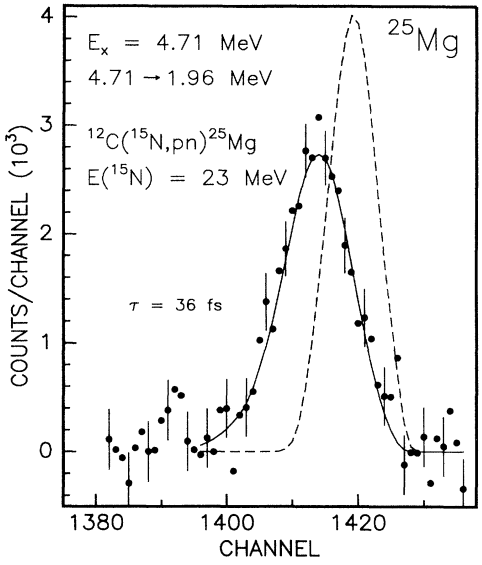

FIG. 2. As for Fig. 1, but for the 4.71-MeV (4.71 → 1.96 MeV transition) ^{25}Mg state. The Monte Carlo simulation is for the lifetime 36 fs; τ(4.06) = 36 ± 4 fs.

ing to the 4.06 → 0 MeV transition was found to be due to the 2.08 ps feeding from the 5.46-MeV state. The 5.46-MeV state has previously been reported to decay via a 100% branch to the 3.41 MeV state.[2,4] The present values for the branching ratios are 91±2% (5.46 → 3.41) and 9.0±0.5% (5.46 → 4.06). The new branching ratios are in agreement with the predictions of the USD shell model.[4]

Near the experimental line shape of the 3967-keV line there was found a stopped peak, which corresponds to the γ-ray energy of 4107 keV. Of the known transitions in ^{25}Mg this can only be due to the 8.82 → 4.71 MeV transition (100% branch, Ref. 4). Observation of the stopped component in the 2747-keV line shape (4.71 → 1.96 MeV transition) due to the 8.82 → 4.71 → 1.96 cascade confirmed this assignment.

C. The ^{24}Mg(p,γ)^{25}Al reaction study

The DSA measurements were performed with a detector at angles 0° and 90° to the beam direction and a target-detector distance of 5.5 cm. A shield of 3 mm lead between the target and the detector was applied to reduce the intensity of low-energy γ rays and x rays. The corrections for solid-angle attenuation of the observed Doppler

TABLE III. The feeding cascades and fractions for the ^{25}Mg levels observed in the ^{12}C(^{15}N,pn)^{25}Mg reaction measurements.

E_x (MeV)	Feeding cascade	Feeding fraction (%)[a] at E(^{15}N) (MeV) 23	27
4.06	prompt	90(2)	80(3)
	9.00→5.25→4.06	1(1)	3(2)
	5.25→4.06	9(2)	17(3)
4.71	prompt	93(3)	62(3)
	8.02→4.71	7(3)	38(3)
5.25	prompt	87(2)	85(2)
	9.00→5.25	13(2)	15(2)

[a]The feeding fraction is defined as the ratio of the feeding intensity to the total decay intensity of the state. The uncertainties given in the parentheses were taken into account in the uncertainties of the deduced lifetimes values.

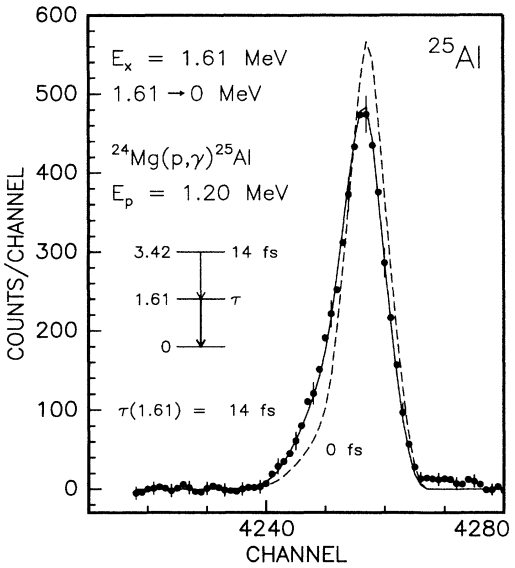

FIG. 3. As for Fig. 1, but for the 1.61-MeV ^{25}Al state. The Monte Carlo simulations for two different lifetimes are shown.

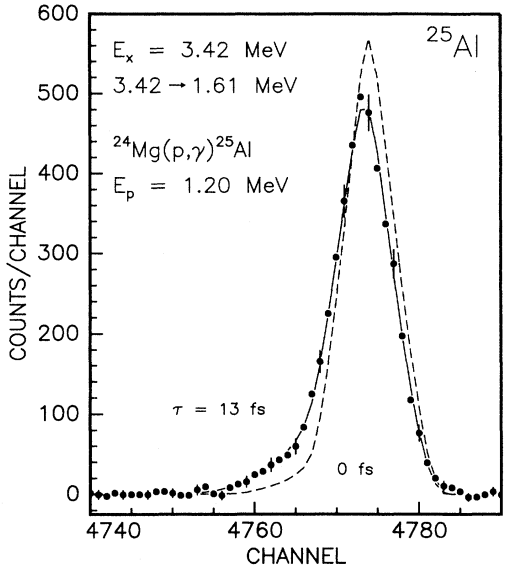

FIG. 5. As for Fig. 3, but for the 3.42-MeV state.

shifts were taken into account by the use of primary γ-ray transitions at the E_p = 1483- and 1654-keV resonances. The accumulated charge for the γ-ray spectra varied between 0.2 and 1.2 C, depending on the strength of the resonance used.

DSA measurements through the reaction ^{24}Mg$(p,\gamma)^{25}$Al are feasible only for the levels below the excitation energy of E_x = 4.2 MeV. At the corresponding bombarding energy (E_p = 2010 keV), the $(p,p'\gamma)$ reaction dominates the exit channel and the strong 1369-keV γ-ray line contaminates the spectra. Below E_x = 4.2 MeV, 13 excited states are known in ^{25}Al (Ref. 2). Among them there are only 4 bound states, E_x = 0.45, 0.94, 1.61, and 1.79 MeV. The long lifetimes of the 0.45 (3.3 ns, Ref. 2) and 0.94 MeV (6.2 ps, Ref. 2) levels, cannot be measured with the present technique. The unbound state at E_x = 2.72 MeV has not been observed as a resonance state in the ^{24}Mg$(p,\gamma)^{25}$Al reaction.

On the basis of the proper γ-decay schemes[2] and γ-ray yields high enough for DSA measurements with im-

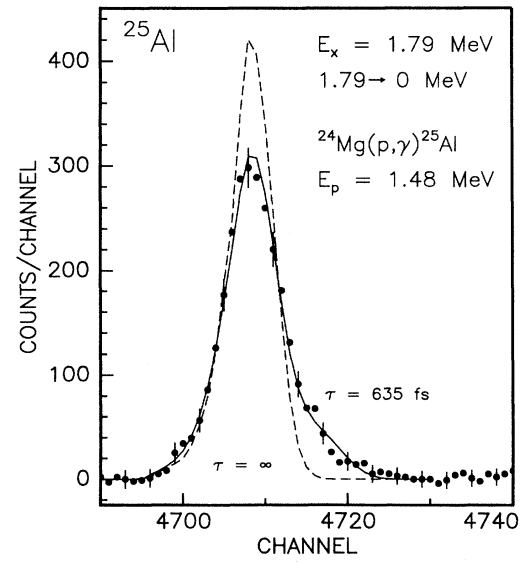

FIG. 4. As for Fig. 3, but for the 1.79-MeV state.

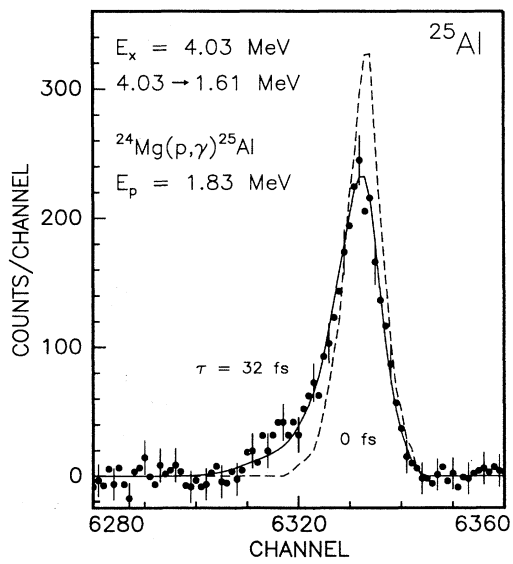

FIG. 6. As for Fig. 3, but for the 4.03-MeV state.

TABLE IV. Summary of the lifetimes in ^{25}Al obtained in the present work and comparison with the previously measured lifetime values.

E_x (MeV)	E_p (MeV)	$F(\tau)$[a] (%)	τ[b] (fs)	τ[c](fs) adopted	τ (fs) (previous values) Ref. 28	Ref. 29	Others
1.61	1.20	65.6±1.9	14±2	14±3	$15\pm^{8}_{5}$	$28\pm^{8}_{6}$	
	1.65	60.2±2.0	15±4				
	1.83	58.1±2.0	$15\pm^{9}_{7}$				
1.79	1.48	7.7±0.8	635±30	635±100	$490\pm^{160}_{90}$	$800\pm^{400}_{200}$	$500\pm^{300}_{200}$[d]
							$550\pm^{100}_{70}$[e]
2.72	1.65	18.9±0.8	300±15	300±45	$270\pm^{130}_{80}$	$450\pm^{100}_{80}$	$450\pm^{100}_{80}$[e]
3.42	1.20	81.5±1.5	13.3±0.6	13.3±2.0	<10	$10\pm^{6}_{5}$	10±6[f]
4.03	1.83	67±4	32±4	32±6			24±5[f]
							22±6[g]

[a]Values have not been corrected for delayed feedings.
[b]Values given are corrected for feedings and are based on the $F(\tau)$ value and on the line-shape analysis. Only statistical errors are shown.
[c]Values include the uncertainty in the experimental stopping power.
[d]Reference 30.
[e]Reference 31.
[f]Reference 32.
[g]Reference 33.

planted targets, the E_p = 1201, 1483, 1654, and 1828-keV resonances were selected for the DSA measurements. Figs. 3–6 show portions of the γ-ray spectra from the DSA measurements of the 1.61-, 1.79-, 3.42-, and 4.03-MeV states, respectively. The summary of the DSA measurements is given in Table IV. The $F(\tau)$ values shown in the table are averages from at least two sets of measurements. The DSA analysis of the experimental $F(\tau)$ values was carried out using the MC method in the simulations of the γ-ray peaks.[7–12] Corrections to the quoted $F(\tau)$ values for delayed feedings from the resonance state were taken into account in the deductions of the lifetime values to the 1.61 MeV state populated through the E_p = 1201 (E_x = 3.42 MeV) and 1828 keV (E_x = 4.03 MeV) resonances. The contamination due to the 1611.8-keV γ-ray transition in ^{25}Mg following the 0.84% β^+-decay branch (Ref. 2) from the ^{25}Al ground state to the third excited ^{25}Mg state was sufficiently resolved in the DSA measurements of the 1612.5-keV γ ray in ^{25}Al. The lifetime of the unbound state at E_x = 2.72 MeV could be measured by employing the 9.6% branch in the decay of the E_p = 1654-keV resonance.

The branching ratios for the DSA analysis were determined from the spectra measured with the 20% efficient HPGe detector located at 130° to the beam direction to monitor the γ-ray yield during the DSA measurements. The detector-target distance was 7.5 cm. The measurements were repeated with the new 20% efficient HPGe detector located at 55° to the beam and at a distance of 3 cm from the target. Branching ratios were also measured for the E_p = 1623 keV resonance. The branching ratios are given in Table V. In general the results are in agreement with the earlier ones. At E_p = 1654 keV the γ peak assigned earlier[2] to the transition from the E_x = 3.86 MeV resonance level to the E_x = 0.45 MeV state is a contamination due to the tail of the broad (Γ = 36 keV) resonance at E_p = 1623 keV, like the contaminations due to the transitions to the E_x = 0.94 and E_x = 2.49 MeV states. The contaminations were determined from the off-resonance measurement at E_p = 1643 keV. At the E_p = 1828 keV resonance, a weak (1%) transition to the E_x = 3.42 MeV level was found. The about 9% transition to the first excited state observed also in the off-resonance spectrum, measured at E_p = 1818 keV, is due to the direct capture.[36]

D. Comparison with previous results

The previous lifetime results of the states in ^{25}Mg and ^{25}Al along with our measurements are summarized in Tables II and IV, respectively. The experimental conditions

of the present and previous DSA measurements of ^{25}Mg and ^{25}Al are shown in Tables VI and VII, respectively.

It is worth noting that systematically shorter lifetime values are obtained by the use of the large-angle scattering correction of Blaugrund[37] than values obtained in the present realistic MC simulations. The systematic error increases with increasing lifetime value. The attenuation factor $F(\tau) = 10\%$ of the $\beta = 0.002$ ^{25}Al recoils in Ta, corresponds to the lifetime values of 400 and 600 fs according to Blaugrund's approximation and the MC simulation, respectively. The longer lifetime value of the 1.79-MeV state than obtained in previous measurements, is most likely due to the use of the MC simulation.

When deducing the adopted lifetime values for the calculation of the $M1$ and $E2$ matrix elements to be discussed in Sec. IV, the procedure used in our earlier works

TABLE V. The γ-ray decay of bound and resonance states in ^{25}Al, as obtained in the present work and comparison with the previous values.

E_p (keV)	E_i (MeV)	E_f (MeV)	$2J_i^a$	$2J_f^a$	Branching ratio (%) Present	Previous values Ref. 34	Ref. 30	Ref. 28	Others
	0.45	0	1	5	100	100	100	100	100[h]
	0.94	0	3	1	44±2	38±6	46±3	39±4	43±4[h]
		0.45		5	56±2	60±9	54±3	61±4	57±6[h]
	1.61	0	7	5	100	>93		100	
	1.79	0	5	5	22±2	25±4	26±2	22±3	22±2[h]
		0.45		1	38±2	48±7	33±3	38±3	31±3[h]
		0.94		5	40±2	27±4	41±2	40±3	47±5[h]
	2.72	0	7	5	6.7±1.5	10±2			<7[h], 8±6[i]
		0.94		3	75.3±4	60±12	>70		72[h], 63±10[i]
		1.79		5	18±2	15±3[b]			14[h], 29±14[i]
1201	3.42	0	9	5	15±1	2.0±0.5		16±4	
		1.61		7	85±3	3±1[c]		84±4	
1484	3.70	0	7^-	5	27±2	16±2	27±2	32±4	30±3[h]
		1.79		5	71±3	65±10[d]	70±4	65±4	68±7[h]
		2.72		7	2.0±0.3		3.0±0.2	3±2	2.0±0.3[h]
1623	3.82	0.45	1^-	1	25±2	20±3		31±5	
		0.94		1	68±3	32±5		61±5	
		2.49		1	7±1	5±1[e]		8±5	
1654	3.86	0	5	5	6.4±1.0	10±2		12±3	8[i]
		0.94		1	66.8±3.5	28±4		63±4	62[i]
		1.61		7	2.4±0.3	8±1		2±2	4[i]
		1.79		5	5.1±0.4	4.0±0.5		6±3	4[i]
		2.49		1	< 0.4	18±3			
		2.67		3	9.0±0.7	10±1		9±3	12[i]
		2.72		7	9.6±0.7	8±1		8±3	5[i,j]
		3.06		3^-	0.7±0.1	4.0±0.5[f]			
1828	4.03	0	9	5	50±3	35±5			60±10[k]
		1.61		7	49±3	7±1[g]			40±10[k]
		3.42		9	1.0±0.5				

[a] If not denoted the parity is positive.
[b] (5±1)% to the 0.45 MeV state.
[c] (2.0±0.5)% to 0.45, (81±20)% to 1.79, (5.0±1.3)% to 2.49 and (7.0±1.5)% to 2.67 MeV state.
[d] (1.0±0.1)% to 0.45, (0.5±0.1)% to 0.94, (12±2)% to 2.49, (1.0±0.1)% to 3.06 and (4.5±0.7)% to 3.42 MeV state.
[e] (25±4)% to 1.61, (8±1)% to 1.79, (5±1)% to 2.72, (2.0±0.3)% to 3.06 and (3.0±0.5)% to 3.70 MeV state.
[f] (2.0±0.3)% to 0.45 and (8±1)% to 3.70 MeV state.
[g] (8±1)% to 0.45, (2.0±0.3)% to 0.94, (30±5)% to 1.79, (15±2)% to 2.69 and (3.0±0.5)% to 3.82 MeV state.
[h] Reference 31.
[i] Reference 35.
[j] 5% to the 0.45 MeV state.
[k] Reference 33.

TABLE VI. Summary of DSA measurements for lifetimes of the ^{25}Mg levels studied in the present work. If the stopping power from the LSS theory with the large angle scattering corrections by Blaugrund have not been used in the DSA analysis, it is marked in the footnotes.

Work	Reaction	v/c (%)	Slowing-down medium	DSA analysis
Present	^{12}C(^{15}N,pn)	2.7–3.5	Ta + implanted ^{12}C ($20\ \mu g/cm^2$)	a
Ref. 24	^{25}Mg(p,p')	0.36–0.49	evaporated ^{25}Mg ($870\ \mu g/cm^2$)+Au	
Refs. 21, 22	^{25}Mg($p,p'\gamma$)	0.83–1.04	evaporated ^{25}Mg ($600\ \mu g/cm^2$)	b
Ref. 23	^{24}Mg($d,p\gamma$)	0.95–1.13	^{24}Mg foil ($300\ \mu g/cm^2$) + evaporated Au	

[a]Experimental stopping power. Computer simulation of the slowing down.
[b]Electronic stopping power of the LSS theory was corrected by a factor of 0.87. Escape of recoils into vacuum has been taken into account.

was used, e.g., Ref. 12. The weight of a measurement was taken to be $(\Delta\tau)^{-2}$ where $\Delta\tau$ is the quoted uncertainty of the lifetime measurement. In those cases where only a statistical error has been reported in the literature or where no information is available on the DSA analysis, an uncertainty of 20% was added in quadrature for the comparison with the values from those measurements for which the uncertainty due to the stopping power is included. Note that in the cases where the literature data include such an uncertainty, the values obtained without experimental stopping data are still subject to a systematic error. The weighted average values thus obtained are given in Table VIII. The systematic error in all the previous lifetime values due to Blaugrund's approximation is the reason behind the adoption of the present lifetime value of 635 ± 100 fs for the 1.79-MeV state in ^{25}Al. The present lifetime values for the 1.96- and 5.46-MeV states in ^{25}Mg (1010±80 and 2080±190 fs, respectively) were adopted, because of the large uncertainties and scatter of the previously reported lifetime values. In other cases the systematic error in previous results was assumed to be covered by the uncertainty due to the stopping power or large statistical uncertainties and all the known lifetime values were taken into account.

IV. DISCUSSION

Absolute values of the $M1$ and $E2$ matrix elements for transitions between positive-parity states in ^{25}Mg and ^{25}Al are deduced from the lifetimes (as measured in the present experiment and combined with previous results as described above) and the branching and mixing ratios tabulated in Refs. 2, 4, and 38. The experimental matrix element values are presented in Table VIII, in comparison with theoretical absolute values calculated from the full *sd*-shell wave functions of the universal *sd*-shell (USD) Hamiltonian.[13] The USD wave functions have been shown to yield a generally good accounting for spectroscopic features of *sd*-shell states when combined with the appropriate effective operators.[5] The $M1$ and $E2$ transition operators used to calculate the matrix

TABLE VII. Same as for Table VI, but for the ^{25}Al levels studied in the present work.

Work[a]	v/c (%)	Slowing-down medium	DSA analysis
present	0.20–0.25	Ta + implanted ^{24}Mg ($15\ \mu g/cm^2$)	b
Ref. 28	0.17–0.24	Ta + implanted ^{24}Mg ($30\ \mu g/cm^2$)	c
Ref. 30	0.22	Evaporated ^{24}Mg ($30–40\ \mu g/cm^2$) + Ta	d
Ref. 31	0.22–0.24	Evaporated ^{24}Mg ($40\ \mu g/cm^2$) + Ta	d
Ref. 29	0.20–0.24	No details given	d
Ref. 32	0.20–0.25	No details given	d
Ref. 33	0.25	Evaporated ^{24}Mg ($40\ \mu g/cm^2$) + Ta	d,e

[a]The ^{24}Mg(p,γ)^{25}Al reaction has been used in all the cases.
[b]Experimental stopping power. Computer simulation of the slowing down.
[c]In the analysis MgO + 50 at.% of $Mg(OH)_2$ was used as the stopping medium.
[d]Slowing-down in the target backing has not been included.
[e]In the analysis ^{24}Mg + 10 at.% of ^{16}O was used as the stopping medium.

elements listed in Table VIII have been obtained from analyses of a compilation[40] of electromagnetic data for states of $A = 17$–39 nuclei. In these analyses, the one-body densities calculated from the USD wave functions are matched with the corresponding experimental matrix elements and the optimal corrections to the conventional free-nucleon parametrizations of the $M1$ and $E2$ operators are extracted by least-squares fits (see, e.g., Refs. 10 and 12 and references therein). The data set[39] used for determining the $M1$ and $E2$ effective operators con-

TABLE VIII. Magnitudes of experimental and theoretical matrix elements[a] for $M1$ and $E2$ transitions between positive parity states in ^{25}Mg-^{25}Al.

E_i (MeV)	E_f (MeV)	$2J_i$	$2J_f$	τ (fs)	Branching ratio (%)	Mixing ratio $\delta(E2/M1)$	$\lvert M(M1)\rvert$ (μ_N)[b] Expt.	*SM*	$\lvert M(E2)\rvert$ $(e\,\mathrm{fm}^2)$[b] Expt.	*SM*
^{25}Mg:										
1.96	0	5	5	1010±80	27.0±0.4	0.58±0.07	0.095±0.005	0.123	3.4±0.3	4.55
	0.58		1		42.5±0.6	0.34±0.25[c]			19±2	20.7
	0.97		3		30.5±0.5	0.25±0.02	0.316±0.013	0.236	9.6±0.8	11.5
3.41	0	9	5	10.2±0.6	19.0±1.0				18.2.±0.7	20.2
	1.61		7		81.0±1.0	0.14±0.02	2.77±0.08	2.70	26±4	24.7
3.91	0	5	5	9±3	11.0±1.0		0.26±0.05	0.165	8.1±1.4	4.50
	0.97		3		66±2	0.02±0.05	1.0±0.2	0.956	0.81±2.04	1.85
	2.74		7		13.0±1.0		1.8±0.3	1.48	180±30	2.56
	2.80		3		10.0±1.0		1.7±0.3	1.34	181±32	11.3
4.06	0	9	5	80±6	60.0±1.0				7.5±0.3	4.27
	1.61		7		39.0±1.0	0.49±0.08	0.53±0.03	1.34	9.4±1.3	17.5
	3.41		9		1.0±0.2		0.68±0.08	1.26	92±10	19.6
4.71	1.96	9	5	36±4	94.0±1.0				37±2	31.0
	2.74		7		6.0±1.0		0.36±0.04	0.209	21±2	9.79
5.25	1.61	11	7	22±3	38±3	0.07±0.09[c]			18±2	19.4
	2.74		7		14±2				25±2	13.8
	3.41		9		25±2	−0.14±0.09	1.10±0.09	2.02	10±6	16.5
	4.06		9		23.0±1.0	0.052±0.058	2.05±0.15	1.41	11±12	23.5
5.46	3.41	13	9	2080±190	91±2	-0.02±0.02[c]			11.7±0.5	9.44
	4.06		9		9.0±0.5				9.5±0.5	7.52
5.52	0	5	5	67±8	22.0±1.0	−0.07±0.10	0.081±0.005		0.12±0.18	2.27
	1.61		7		30±2	−0.15±0.05	0.158±0.011		0.73±0.24	3.59
	1.96		5		16±2	0.01±0.09	0.135±0.012		0.04±0.40	8.20
	2.80		3		12±2		0.17±0.02		7.7±0.8	4.28
5.53	1.61	11	7	8±3	65±3				29±6	15.3
	3.41		9		35±3	0.12±0.06	1.7±0.3	2.16	12±6	14.7
8.02	4.71	13[d]	9	53±3	100		0.60±0.02		23.4±0.6	24.7
^{25}Al:										
1.61	0	7	5	14±3	100	−0.18±0.03	2.8±0.3	2.36	37±7	26.5
1.79	0	5	5	635±100	23.0±1.0	−0.82±0.13	0.128±0.013	0.123	6.2±0.8	7.02
	0.45		1		37.0±1.2				26±2	20.7
	0.94		3		40.0±1.3	−0.170±0.010	0.63±0.05	0.287	14.2±1.4	11.8
2.72	0	7	5	300±45	7.0±1.5		0.074±0.011	0.024	3.2±0.3	2.74
	0.94		3		76±3				31±2	27.2
	1.79		5		17±2	−0.18±0.14	0.50±0.05	0.491	13±9	7.72
3.42	0	9	5	13.3±2.0	15±1				14.0±1.2	18.2
	1.61		7		85±3	−0.14±0.03	2.4±0.2	2.89	23±5	21.7
4.03	0	9	5	32±6	50±3				11.0±1.1	6.66
	1.61		7		49±3		0.71±0.11	1.37	39±4	17.5
	3.42		9		1.0±0.5				180±50	16.3

[a] Except for lifetimes, and for branching ratios in ^{25}Al, the experimental values are based on the previous data taken from Refs. 2, 4, and 38.

[b] If the mixing ratio is unknown, the experimental matrix elements are given for pure multipoles.

[c] $\delta(M3/E2)$.

[d] Spin values $\frac{9}{2}^+$ and $\frac{11}{2}^+$ are also possible (Ref. 4). The $E2$ matrix element values are 5.05 and 2.74 $e\,\mathrm{fm}^2$, respectively.

sisted of the 147 experimental matrix elements from *sd*-shell transitions that have uncertainties of ±10% or less. Theoretical values of $M1$ and $E2$ matrix elements for transitions in ^{25}Mg-^{25}Al calculated with these effective operators (Table VIII) are in very good agreement with the experimental matrix elements.

ACKNOWLEDGMENTS

This work was supported by the Academy of Finland and the Hungarian Academy of Sciences. Prof. B. H. Wildenthal is acknowledged for providing the computer code for the calculations of the electromagnetic transition matrix elements.

[1] A. E. Litherland, H. McManus, E. B. Paul, D. A. Bromley, and H. E. Gove, Can. J. Phys. **36**, 378 (1958).
[2] P. M. Endt and C. van der Leun, Nucl. Phys. **A310**, 1 (1978).
[3] T. Kihm, G. Mairle, P. Grabmayr, K. Knopfle, G. Wagner, B. Bechtold, and L. Friedrich, Z. Phys. A **318**, 205 (1984).
[4] D. M. Headly, R. K. Sheline, S. L. Tabor, U. J. Hüttmeier, C. J. Gross, E. F. Moore, B. H. Wildenthal, H. R. Weller, R. M. Whitton, and I. Ragnarsson, Phys. Rev. C **38**, 1698 (1988).
[5] B. A. Brown and B. H. Wildenthal, Annu. Rev. Nucl. Part. Sci. **38**, 29 (1988).
[6] G. Andersson *et al.*, Nucl. Phys. **A268**, 205 (1976).
[7] J. Keinonen, in *Capture γ-Ray Spectroscopy and Related Topics-1984*, edited by S. Raman (AIP, New York, 1985), p. 557.
[8] P. Tikkanen, J. Keinonen, V. Karttunen, and A. Kuronen, Nucl. Phys. **A456**, 337 (1986).
[9] P. Tikkanen, J. Keinonen, R. Lappalainen, and B. H. Wildenthal, Phys. Rev. C **36**, 32 (1987).
[10] J. Keinonen, P. Tikkanen, A. Kuronen, Á. Z. Kiss, E. Somorjai, and B. H. Wildenthal, Nucl. Phys. **A493**, 124 (1989).
[11] P. Tikkanen, J. Keinonen, K. Arstila, A. Kuronen, and B. H. Wildenthal, Phys. Rev. C **42**, 581 (1990).
[12] P. Tikkanen, J. Keinonen, A. Kuronen, Á. Z. Kiss, E. Koltay, É. Pintye, and B. H. Wildenthal, Nucl. Phys. **A517**, 176 (1990).
[13] B. H. Wildenthal, Part. Nucl. Phys. **11**, 5 (1984).
[14] B. A. Brown and B. H. Wildenthal, Nucl. Phys. **A474**, 290 (1987).
[15] J. Lindhard, M. Scharff, and H. E. Schiøtt, Mat. Fys. Medd. Dan. Vid. Selsk. **33** (1963).
[16] W. H. Trzaska, Nucl. Instrum. Methods **A297**, 223 (1990).
[17] J. F. Ziegler, J. P. Biersack, and U. Littmark, in *The Stopping and Range of Ions in Solids*, edited by J. F. Ziegler (Pergamon, New York, 1985), Vol. 1.
[18] A. Luukkainen, J. Keinonen, and M. Erola, Phys. Rev. B **32**, 4814 (1985).
[19] A. Anttila, M. Bister, A. Luukkainen, Á. Z. Kiss, and E. Somorjai, Nucl. Phys. **A385**, 194 (1982).
[20] K. Arstila, J. Keinonen, and P. Tikkanen, Phys. Rev. B **41**, 6117 (1990).
[21] R. W. Ollerhead, D. C. Kean, R. M. Gorman, and M. B. Thomson, Can. J. Phys. **52**, 2329 (1974).
[22] R. W. Ollerhead, D. C. Kean, S. G. T. Leong, C. Doekes, and T. M. R. Meadley, Can. J. Phys. **53**, 123 (1975).
[23] H. Röpke, W. Brendler, P. Betz, V. Glattes, and G. Hammel, Z. Phys. **271**, 59 (1974).
[24] J. F. Sharpey-Schafer, R. W. Ollerhead, and A. J. Ferguson, Can. J. Phys. **46**, 2039 (1968).
[25] Y. Okazaki, K. Hayakawa, K. Nakahara, M. Oyamada, T. Terasawa, and H. Saito, Phys. Lett. **55B**, 373 (1975).
[26] E. W. Lees, C. S. Curran, T. E. Drake, W. A. Gillespie, A. Johnston, and R. P. Singhal, J. Phys. G **2**, 341 (1976).
[27] L. W. Fagg, W. L. Bendel, E. C. Jones, Jr., H. F. Kaiser, and T. F. Godlove, Phys. Rev. **187**, 1384 (1969).
[28] M. Piiparinen, Z. Phys. **252**, 206 (1972).
[29] N. Anyas-Weiss and A. E. Litherland, Bull. Am. Phys. Soc. **13**, 85 (1968).
[30] G. J. McCallum, R. J. Sparks, G. E. Coote, and K. P. Pohl, Can. J. Phys. **49**, 467 (1971).
[31] N. Anyas-Weiss and A. E. Litherland, Can. J. Phys. **47**, 2609 (1969).
[32] N. Anyas-Weiss, A. E. Litherland, and H. Röpke, Phys. Lett. **27B**, 161 (1968).
[33] H. Röpke, N. Anyas-Weiss, and A. E. Litherland, Can. J. Phys. **46**, 2789 (1968).
[34] R. J. van Reenen, Z. B. D. Toit, and W. L. Mouton, Z. Phys. **227**, 326 (1969).
[35] H. E. Gove, A. E. Litherland, and E. Almqvist, Phys. Rev. **111**, 608 (1958).
[36] H. P. Trautvetter and C. Rolfs, Nucl. Phys. **A242**, 519 (1975).
[37] A. E. Blaugrund, Nucl. Phys. **88**, 501 (1966).
[38] D. E. Alburger and E. K. Warburton, Nucl. Phys. **A385**, 474 (1982).
[39] B. H. Wildenthal and J. Keinonen, unpublished.